Supplemental Material for LHCb-PAPER-2019-012

Comparisons to ATLAS Inclusive Jet Measurements

These figures compare results presented in this Letter with published results from ATLAS. Comparisons are made between the results presented here to inclusive midrapidity jet results published in 2011 by ATLAS as noted in the legends. An additional comparison is made to measurements in the isolated photon-jet channel. The relevant ATLAS references are written in the legends of the figures. It is worth noting that the kinematic regions are not exactly the same, so qualitative, rather than quantitative, comparisons of the shapes should be made.

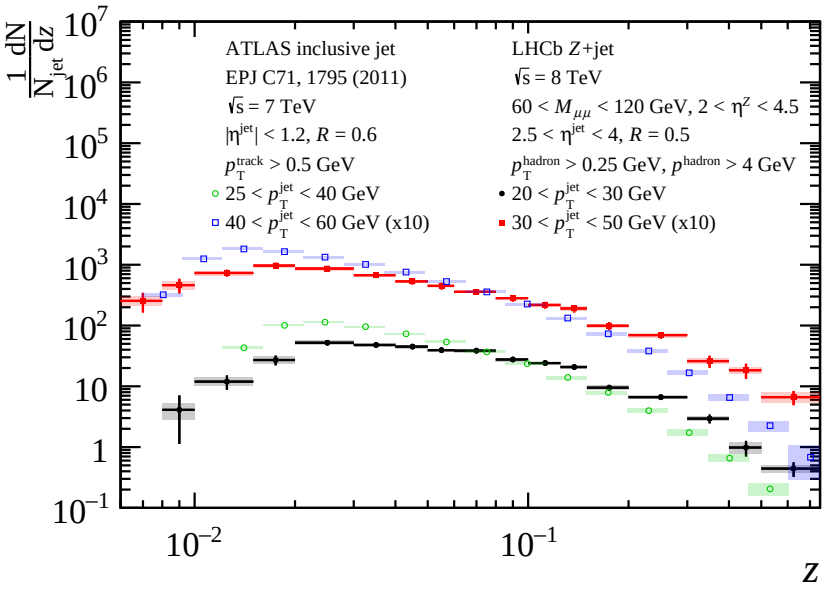

Figure 1: The longitudinal charged hadron-in-jet distributions are compared to measurements from the ATLAS collaboration in the midrapidity inclusive jet channel. Information regarding the kinematic bins for each measurement can be found in the legends.

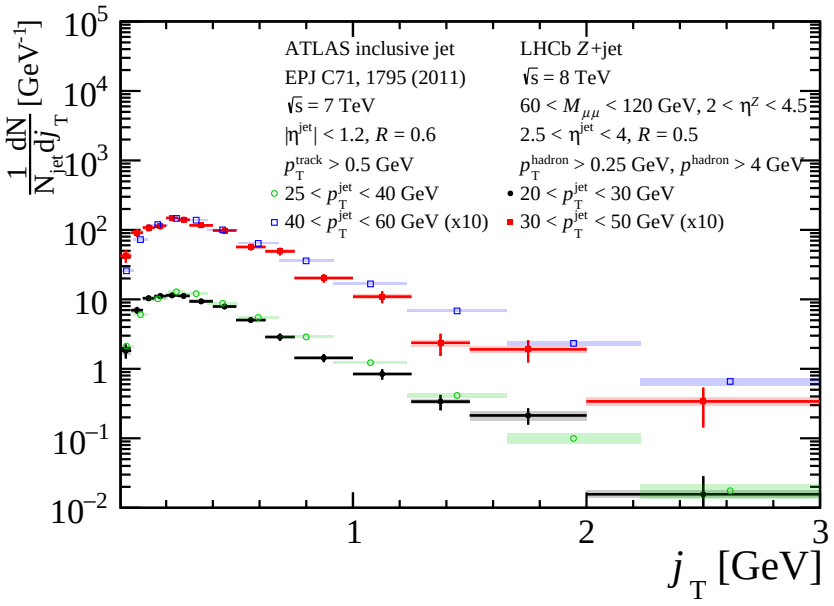

Figure 2: The charged hadron-in-jet momentum transverse to the jet axis distributions are compared to measurements from the ATLAS collaboration in the midrapidity inclusive jet channel. Information regarding the kinematic bins for each measurement can be found in the legends.

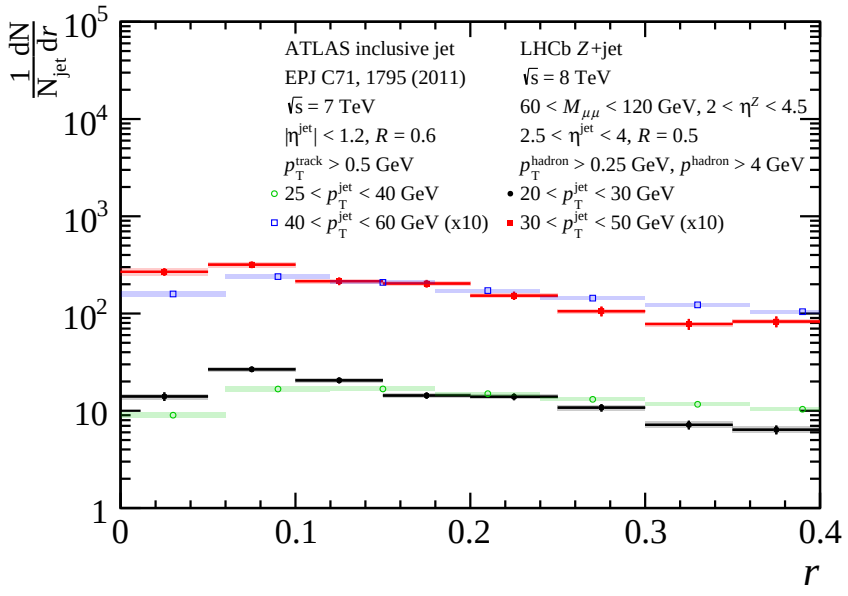

Figure 3: The radial charged hadron-in-jet distributions are compared to measurements from the ATLAS collaboration in the midrapidity inclusive jet channel. Information regarding the kinematic bins for each measurement can be found in the legends.

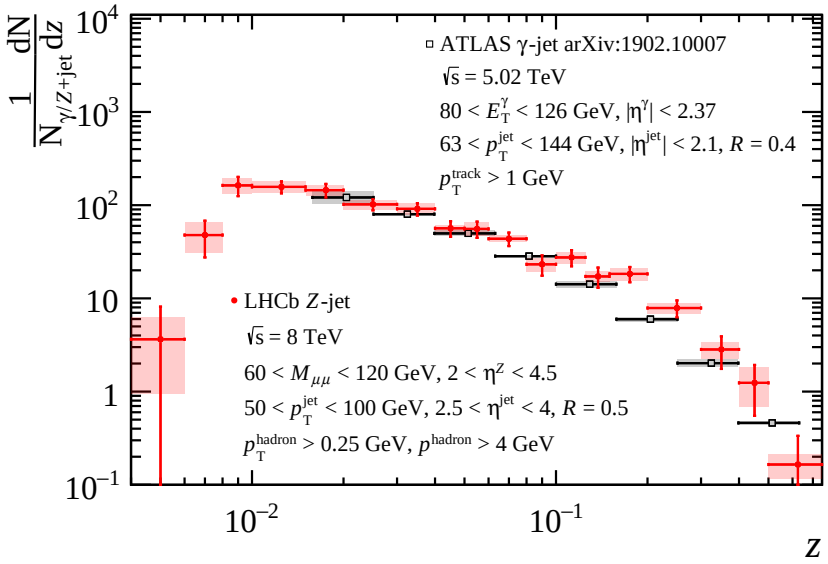

Figure 4: The longitudinal charged hadron-in-jet distributions are compared to measurements from the ATLAS collaboration in the midrapidity isolated photon-jet channel. Information regarding the kinematic bins for each measurement can be found in the legends.

Pythia 8 Comparisons

The Pythia predictions are generated using Pythia 8.175 with the CTEQ6L.1 parton distribution function set and parameter settings displayed in Table ?? and ??. The comparisons of the charged hadron-in-jet fragmentation distributions to the Pythia 8 event generator are shown for each of the jet p_{T} bins in each of the three fragmentation observables in Figs. ??, ??, and ??.

Table 1: Settings used in comparisons between Pythia 8 and these measurements.

General	Multiparton Interactions
SpaceShower:rapidityOrder = off	MultipartonInteractions:bProfile = 1
WeakBosonAndParton:qg2gmZq = on	MultipartonInteractions:ecmRef = 7000
WeakBosonAndParton:qqbar2gmZg = on	MultipartonInteractions:pT0Ref = 2.88
WeakZ0:gmZmode = 2	MultipartonInteractions:ecmPow = 0.238
23:onMode = off	
23:onIfAny = 13	
SigmaProcess:alphaSorder = 2	

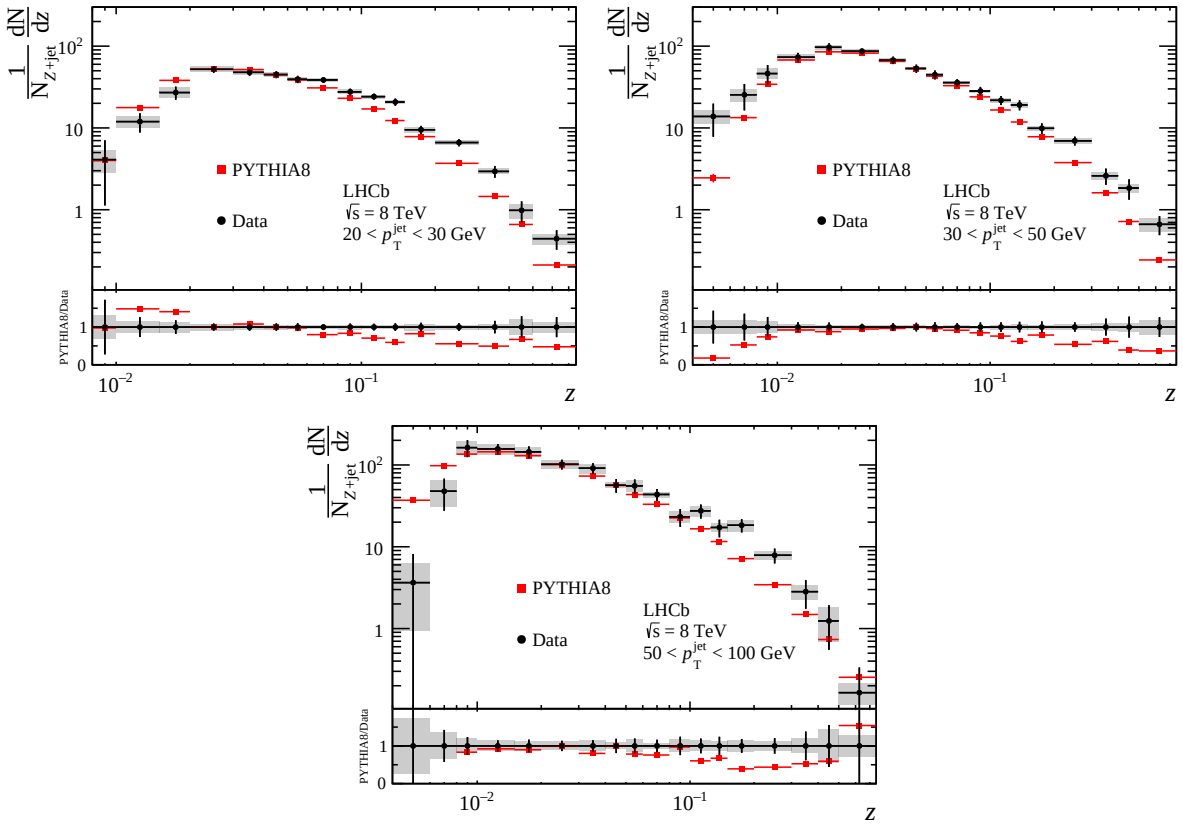

Figure 5: Measured charged hadron-in-jet longitudinal momentum distributions compared to the Pythia 8 event generator in each jet p_{T} bin. The jet p_{T} bins are noted in the corresponding figure.

Table 2: Settings used in comparisons between PYTHIA 8 and these measurements.

String Flavor
StringFlav:mesonUDvector = 0.6
StringFlav:mesonSvector = 0.6
StringFlav:mesonCvector = 3.0
StringFlav:mesonBvector = 3.0
StringFlav:probStoUD = 0.30
StringFlav:probQQtoQ = 0.10
StringFlav:probSQtoQQ = 0.4
StringFlav:probQQ1toQQ0 = 0.05
StringFlav:mesonUDL1S0J1 = 0.0989
StringFlav:mesonUDL1S1J0 = 0.0132
StringFlav:mesonUDL1S1J1 = 0.0597
StringFlav:mesonUDL1S1J2 = 0.0597
StringFlav:mesonSL1S0J1 = 0.0989
StringFlav:mesonSL1S1J0 = 0.0132
StringFlav:mesonSL1S1J1 = 0.0597
StringFlav:mesonSL1S1J2 = 0.0597
StringFlav:mesonCL1S0J1 = 0.0990
StringFlav:mesonCL1S1J0 = 0.0657
StringFlav:mesonCL1S1J1 = 0.2986
StringFlav:mesonCL1S1J2 = 0.2986
StringFlav:mesonBL1S0J1 = 0.0990
StringFlav:mesonBL1S1J0 = 0.0657
StringFlav:mesonBL1S1J1 = 0.2986
StringFlav:mesonBL1S1J2 = 0.2986
StringFlav:etaSup = 1.
StringFlav:etaPrimeSup = 0.4

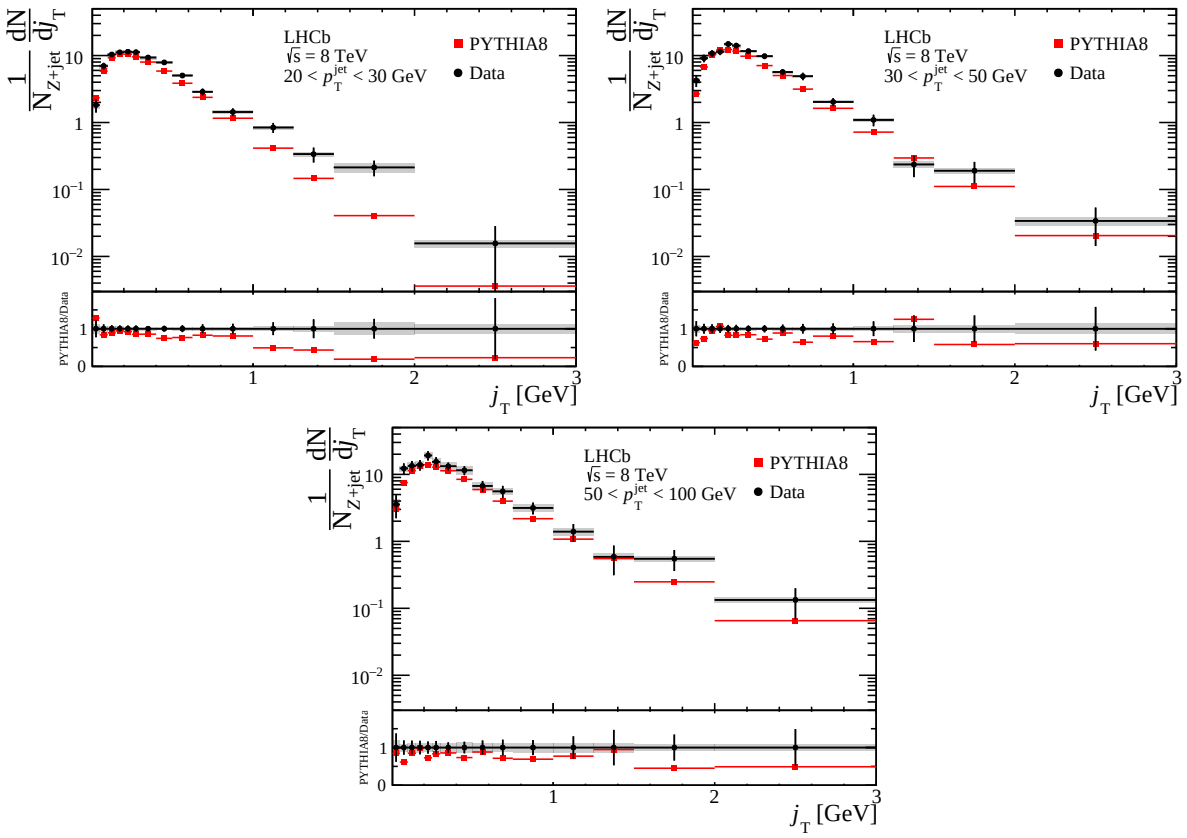

Figure 6: Measured charged hadron-in-jet momentum transverse to the jet axis distributions with respect to the jet axis compared to the PYTHIA 8 event generator in each jet p_{T} bin. The jet p_{T} bins are noted in the corresponding figure.

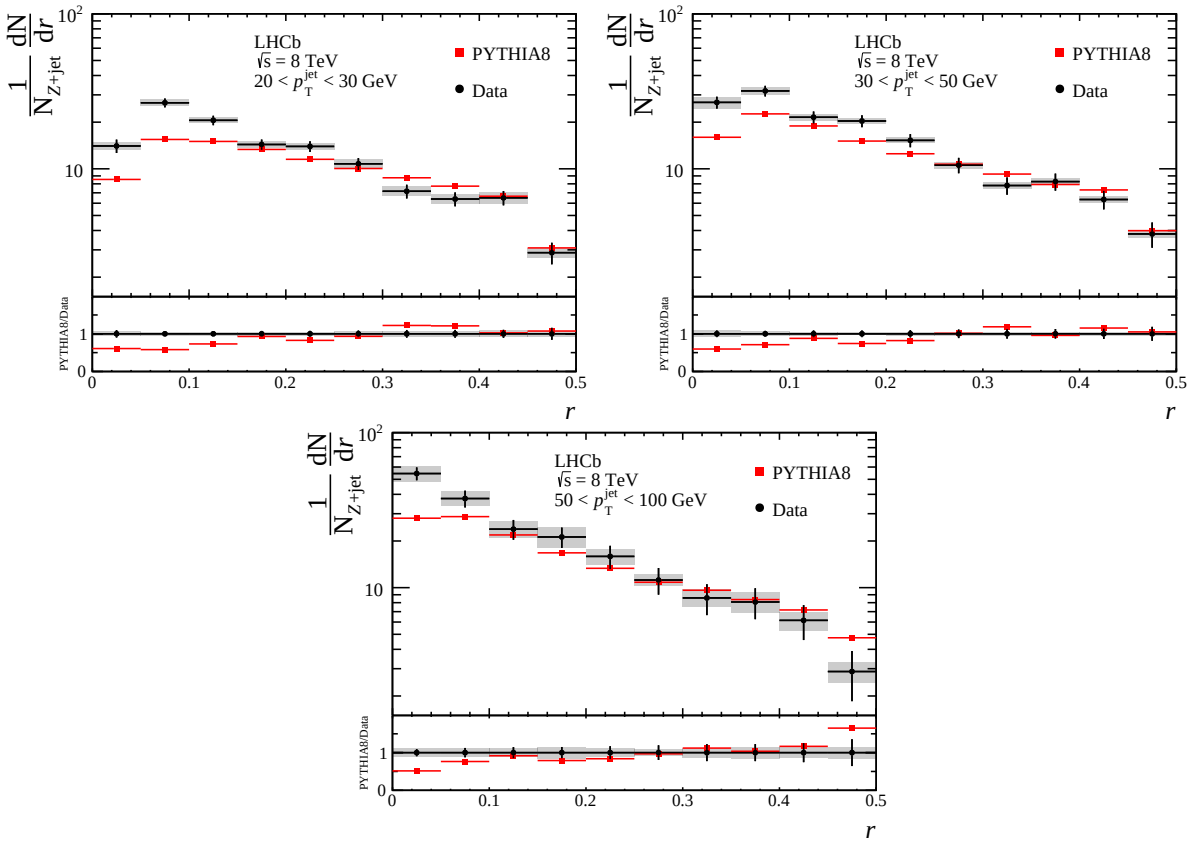

Figure 7: Measured charged hadron-in-jet radial distributions compared to the Pythia 8 event generator in each jet p_{T} bin. The jet p_{T} bins are noted in the corresponding figure.

Numerical Results

The numerical results of the fragmentation distributions are shown in the following tables. The distributions are measured in proton-proton collisions at a center-of-mass energy $\sqrt{s} = 8\,\text{TeV}$. The Z boson is required to have $60 < M_{\mu\mu} < 120\,\text{GeV}$ and $2 < \eta < 4.5$. No selection criterion is placed on the Z p_T so that the distributions can be studied as a function of jet p_T; however, no Z bosons are measured with p_T greater than 100 GeV. The recoiling jet is required to have $2.5 < \eta < 4$ and be nearly back-to-back such that $\Delta\phi_{\text{Z+jet}} \equiv |\phi_\text{Z} - \phi_\text{jet}| > 7\pi/8$. Charged hadrons are measured with $4 < p < 1000\,\text{GeV}$ and $p_\text{T} > 0.25\,\text{GeV}$, and must lie within the jet cone such that $\Delta R < 0.5$ where $\Delta R \equiv \sqrt{(\phi_\text{jet} - \phi_\text{hadron})^2 + (\eta_\text{jet} - \eta_\text{hadron})^2}$.

Table 3: The unfolded charged hadron-in-jet longitudinal momentum distributions for jet p_T $20 < p_\text{T} < 30\,\text{GeV}$. The quantity is shown followed by its statistical uncertainty and lastly by its systematic uncertainty.

z	$(1/N_{Z+\text{jet}})dN/dz$				
0.008 – 0.01	4.10	±	2.97	±	1.27
0.01 – 0.015	11.9	±	3.2	±	1.9
0.015 – 0.02	27.1	±	4.9	±	3.9
0.02 – 0.03	52.1	±	5.0	±	4.4
0.03 – 0.04	47.9	±	4.8	±	3.5
0.04 – 0.05	45.0	±	4.4	±	3.0
0.05 – 0.06	39.3	±	4.0	±	2.1
0.06 – 0.08	38.6	±	3.1	±	2.3
0.08 – 0.1	27.6	±	2.6	±	1.9
0.1 – 0.125	24.1	±	2.2	±	1.3
0.125 – 0.15	20.7	±	2.1	±	1.2
0.15 – 0.2	9.50	±	1.10	±	0.83
0.2 – 0.3	6.63	±	0.68	±	0.43
0.3 – 0.4	2.94	±	0.49	±	0.22
0.4 – 0.5	0.983	±	0.283	±	0.205
0.5 – 0.75	0.443	±	0.119	±	0.065

Table 4: The unfolded charged hadron-in-jet longitudinal momentum distributions for jet p_{T} $30 < p_{\mathrm{T}} < 50\,\mathrm{GeV}$. The quantity is shown followed by its statistical uncertainty and lastly by its systematic uncertainty.

z	$(1/N_{Z+\mathrm{jet}})dN/dz$				
0.004 – 0.006	13.8	±	6.0	±	2.6
0.006 – 0.008	25.4	±	9.1	±	4.6
0.008 – 0.01	46.2	±	12.4	±	7.1
0.01 – 0.015	73.2	±	9.6	±	6.2
0.015 – 0.02	96.9	±	11.7	±	6.6
0.02 – 0.03	86.7	±	7.6	±	4.9
0.03 – 0.04	67.4	±	7.1	±	3.5
0.04 – 0.05	53.3	±	6.1	±	2.7
0.05 – 0.06	44.8	±	5.7	±	2.0
0.06 – 0.08	35.8	±	3.7	±	1.7
0.08 – 0.1	28.3	±	3.5	±	1.1
0.1 – 0.125	21.8	±	2.7	±	1.4
0.125 – 0.15	19.1	±	2.7	±	1.5
0.15 – 0.2	9.90	±	1.47	±	0.64
0.2 – 0.3	6.96	±	0.87	±	0.56
0.3 – 0.4	2.60	±	0.59	±	0.28
0.4 – 0.5	1.84	±	0.52	±	0.22
0.5 – 0.75	0.663	±	0.175	±	0.125

Table 5: The unfolded charged hadron-in-jet longitudinal momentum distributions for jet p_{T} $50 < p_{\mathrm{T}} < 100\,\mathrm{GeV}$. The quantity is shown followed by its statistical uncertainty and lastly by its systematic uncertainty.

z	$(1/N_{Z+\mathrm{jet}})dN/dz$				
0.004 – 0.006	3.64	±	4.51	±	2.69
0.006 – 0.008	47.8	±	20.3	±	17.0
0.008 – 0.01	163	±	38	±	31
0.01 – 0.015	157	±	23	±	22
0.015 – 0.02	145	±	24	±	19
0.02 – 0.03	102	±	14	±	12
0.03 – 0.04	91.3	±	13.9	±	12.9
0.04 – 0.05	56.5	±	10.7	±	4.8
0.05 – 0.06	55.6	±	11.0	±	9.1
0.06 – 0.08	43.6	±	7.2	±	3.5
0.08 – 0.1	23.2	±	5.7	±	3.9
0.1 – 0.125	27.5	±	5.4	±	3.9
0.125 – 0.15	17.2	±	4.2	±	2.2
0.15 – 0.2	18.3	±	3.4	±	2.9
0.2 – 0.3	7.88	±	1.63	±	0.99
0.3 – 0.4	2.83	±	1.08	±	0.56
0.4 – 0.5	1.24	±	0.69	±	0.56
0.5 – 0.75	0.165	±	0.170	±	0.048

Table 6: The unfolded charged hadron-in-jet momentum transverse to the jet axis distributions for jet p_{T} $20 < p_{\mathrm{T}} < 30\,\mathrm{GeV}$. The quantity is shown followed by its statistical uncertainty and lastly by its systematic uncertainty. Units are GeV for j_T and GeV^{-1} for the normalized multiplicities and their uncertainties.

j_T	$(1/N_{Z+\mathrm{jet}})dN/dj_T$		
0.0 – 0.05	1.82 ±	0.41 ±	0.22
0.05 – 0.1	6.98 ±	0.80 ±	0.52
0.1 – 0.15	10.4 ±	1.0 ±	0.7
0.15 – 0.2	11.2 ±	1.0 ±	0.8
0.2 – 0.25	11.4 ±	1.0 ±	0.6
0.25 – 0.3	11.2 ±	1.0 ±	0.6
0.3 – 0.4	9.35 ±	0.68 ±	0.55
0.4 – 0.5	7.89 ±	0.63 ±	0.38
0.5 – 0.625	5.04 ±	0.46 ±	0.29
0.625 – 0.75	2.87 ±	0.34 ±	0.15
0.75 – 1	1.44 ±	0.19 ±	0.09
1 – 1.25	0.842±	0.140±	0.056
1.25 – 1.5	0.337±	0.084±	0.027
1.5 – 2	0.213±	0.056±	0.035
2 – 3	0.015±	0.013±	0.002

Table 7: The unfolded charged hadron-in-jet momentum transverse to the jet axis distributions for jet p_{T} $30 < p_{\mathrm{T}} < 50\,\mathrm{GeV}$. The quantity is shown followed by its statistical uncertainty and lastly by its systematic uncertainty. Units are GeV for j_T and GeV^{-1} for the normalized multiplicities and their uncertainties.

j_T	$(1/N_{Z+\mathrm{jet}})dN/dj_T$		
0.0 – 0.05	4.24 ±	0.85 ±	0.45
0.05 – 0.1	9.12 ±	1.20 ±	0.61
0.1 – 0.15	10.8 ±	1.3 ±	0.7
0.15 – 0.2	11.4 ±	1.3 ±	0.6
0.2 – 0.25	14.9 ±	1.5 ±	0.8
0.25 – 0.3	14.1 ±	1.4 ±	0.8
0.3 – 0.4	11.6 ±	1.0 ±	0.6
0.4 – 0.5	9.79 ±	0.94 ±	0.45
0.5 – 0.625	5.67 ±	0.62 ±	0.28
0.625 – 0.75	4.91 ±	0.62 ±	0.28
0.75 – 1	2.03 ±	0.28 ±	0.11
1 – 1.25	1.09 ±	0.21 ±	0.07
1.25 – 1.5	0.236±	0.083±	0.026
1.5 – 2	0.191±	0.067±	0.020
2 – 3	0.034±	0.020±	0.005

Table 8: The unfolded charged hadron-in-jet momentum transverse to the jet axis for jet p_{T} $50 < p_{\mathrm{T}} < 100\,\mathrm{GeV}$. The quantity is shown followed by its statistical uncertainty and lastly by its systematic uncertainty. Units are GeV for j_T and GeV^{-1} for the normalized multiplicities and their uncertainties.

j_T	$(1/N_{Z+\mathrm{jet}})dN/dj_T$				
0.0 – 0.05	3.55	±	1.30	±	0.70
0.05 – 0.1	12.3	±	2.3	±	1.3
0.1 – 0.15	13.4	±	2.5	±	1.7
0.15 – 0.2	13.9	±	2.5	±	1.7
0.2 – 0.25	19.2	±	3.1	±	2.1
0.25 – 0.3	15.4	±	2.7	±	1.8
0.3 – 0.4	13.2	±	1.8	±	1.7
0.4 – 0.5	11.5	±	1.8	±	1.7
0.5 – 0.625	6.72	±	1.30	±	0.83
0.625 – 0.75	5.57	±	1.20	±	0.66
0.75 – 1	3.16	±	0.63	±	0.40
1 – 1.25	1.40	±	0.42	±	0.19
1.25 – 1.5	0.589	±	0.280	±	0.072
1.5 – 2	0.550	±	0.190	±	0.051
2 – 3	0.133	±	0.066	±	0.012

Table 9: The unfolded charged hadron-in-jet radial distributions for jet p_{T} $20 < p_{\mathrm{T}} < 30\,\mathrm{GeV}$. The quantity is shown followed by its statistical uncertainty and lastly by its systematic uncertainty.

r	$(1/N_{Z+\mathrm{jet}})dN/dr$				
0 – 0.05	14.0	±	1.4	±	0.9
0.05 – 0.1	26.7	±	1.8	±	1.4
0.1 – 0.15	20.6	±	1.4	±	1.0
0.15 – 0.2	14.4	±	1.1	±	0.7
0.2 – 0.25	13.9	±	1.1	±	0.8
0.25 – 0.3	10.8	±	0.9	±	0.7
0.3 – 0.35	7.17	±	0.73	±	0.52
0.35 – 0.4	6.38	±	0.66	±	0.48
0.4 – 0.45	6.50	±	0.69	±	0.60
0.45 – 0.5	2.88	±	0.46	±	0.22

Table 10: The unfolded charged hadron-in-jet radial distributions for jet p_{T} $30 < p_{\mathrm{T}} < 50\,\mathrm{GeV}$. The quantity is shown followed by its statistical uncertainty and lastly by its systematic uncertainty.

r	$(1/N_{Z+\mathrm{jet}})dN/dr$				
0 – 0.05	26.8	±	2.4	±	2.3
0.05 – 0.1	31.8	±	2.5	±	2.0
0.1 – 0.15	21.5	±	1.9	±	1.2
0.15 – 0.2	20.3	±	1.8	±	1.0
0.2 – 0.25	15.3	±	1.5	±	0.8
0.25 – 0.3	10.6	±	1.2	±	0.6
0.3 – 0.35	7.80	±	1.00	±	0.43
0.35 – 0.4	8.27	±	1.04	±	0.44
0.4 – 0.45	6.34	±	0.87	±	0.34
0.45 – 0.5	3.80	±	0.70	±	0.24

Table 11: The unfolded charged hadron-in-jet radial distributions for jet p_{T} $50 < p_{\mathrm{T}} < 100\,\mathrm{GeV}$. The quantity is shown followed by its statistical uncertainty and lastly by its systematic uncertainty.

r	$(1/N_{Z+\mathrm{jet}})dN/dr$				
0 – 0.05	54.5	±	5.2	±	6.2
0.05 – 0.1	37.6	±	4.7	±	4.3
0.1 – 0.15	23.9	±	3.5	±	2.9
0.15 – 0.2	21.2	±	3.2	±	3.3
0.2 – 0.25	15.9	±	2.7	±	1.8
0.25 – 0.3	11.2	±	2.2	±	1.0
0.3 – 0.35	8.58	±	1.94	±	1.12
0.35 – 0.4	8.08	±	1.83	±	1.23
0.4 – 0.45	6.15	±	1.56	±	0.87
0.45 – 0.5	2.88	±	1.03	±	0.44

Covariance Matrices

The covariance matrices for the three observables are shown in the following figures.

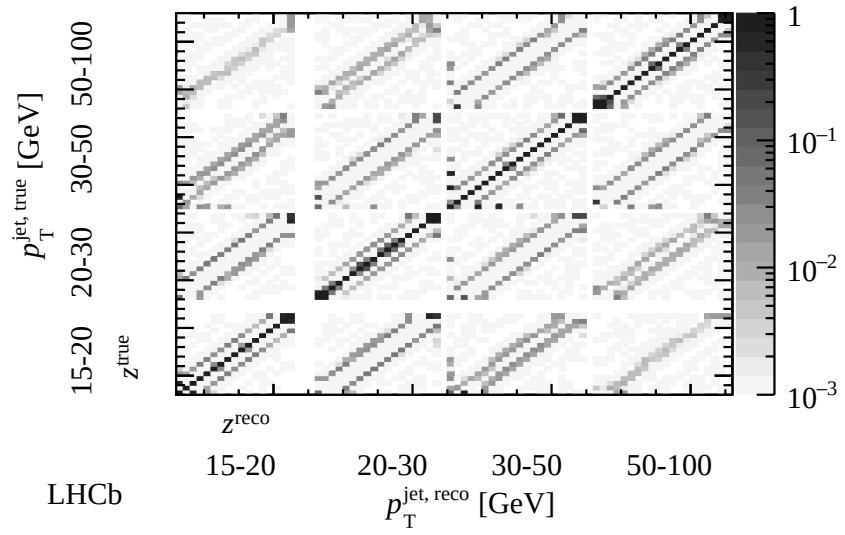

Figure 8: The covariance matrix for the longitudinal momentum fraction z is shown in the four jet p_{T} bins measured, where the lowest jet p_{T} bin shown here is only included for the purpose of the two-dimensional unfolding.

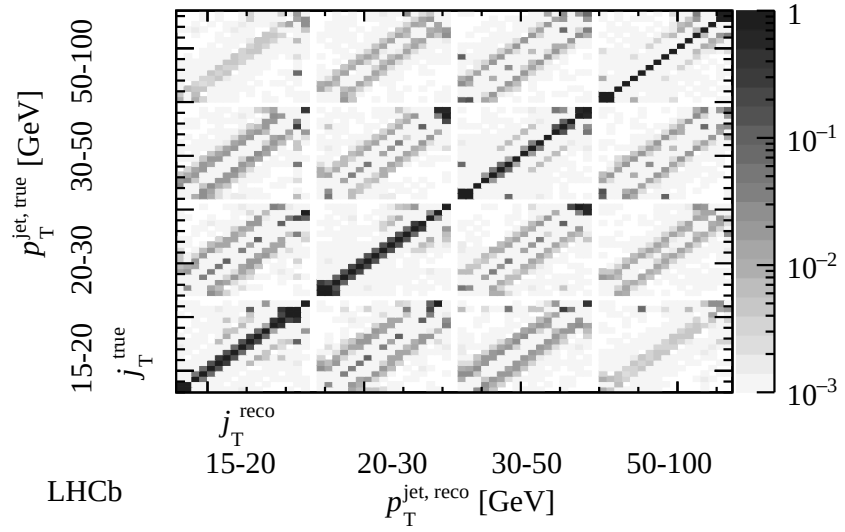

Figure 9: The covariance matrix for the charged hadron-in-jet momentum transverse to the jet axis j_T is shown in the four jet p_{T} bins measured, where the lowest jet p_{T} bin shown here is only included for the purpose of the two-dimensional unfolding.

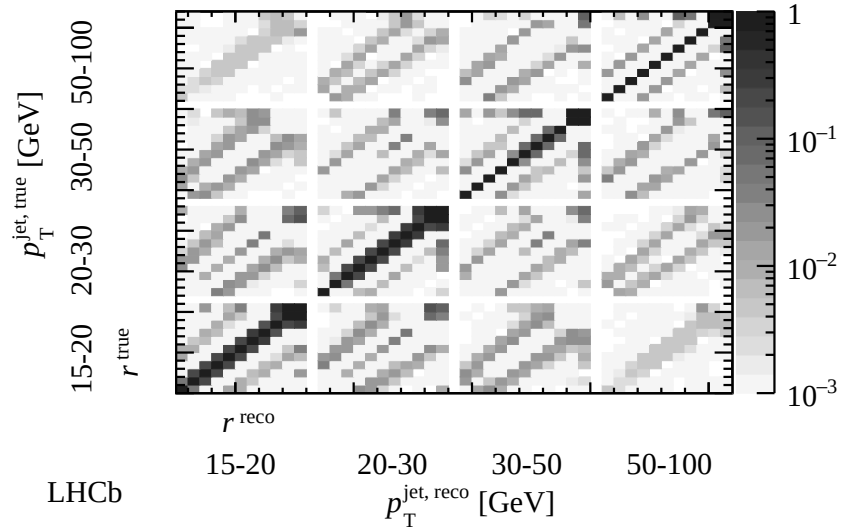

Figure 10: The covariance matrix for the radial profile r is shown in the four jet p_{T} bins measured, where the lowest jet p_{T} bin shown here is only included for the purpose of the two-dimensional unfolding.

PYTHIA Partonic Fraction Studies

The figures below show a short PYTHIA 8 study showing the partonic fractions that contribute at leading order to forward Z+jet production and midrapidity inclusive jet production. Note that for midrapidity inclusive jet production, there are two additional leading order diagrams that contribute less than a few percent that are excluded from the figure.

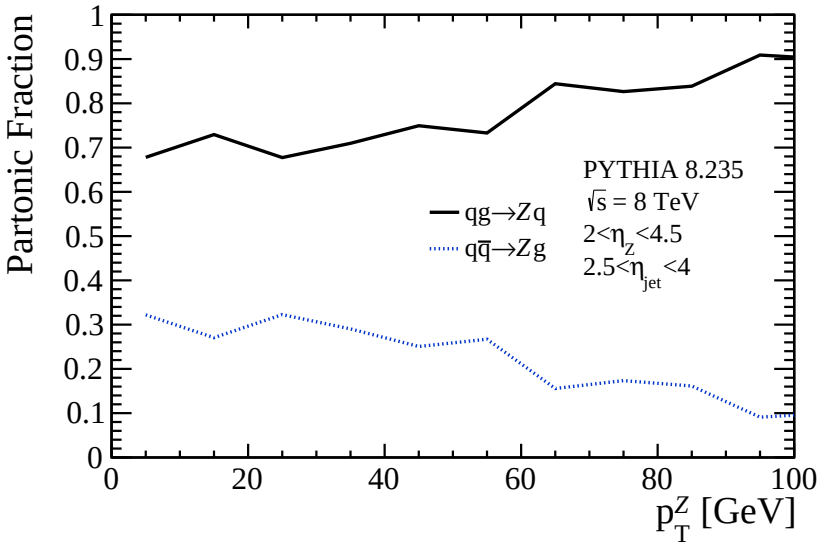

Figure 11: The partonic fractions that contribute to forward Z+jet production at leading order, according to PYTHIA 8.

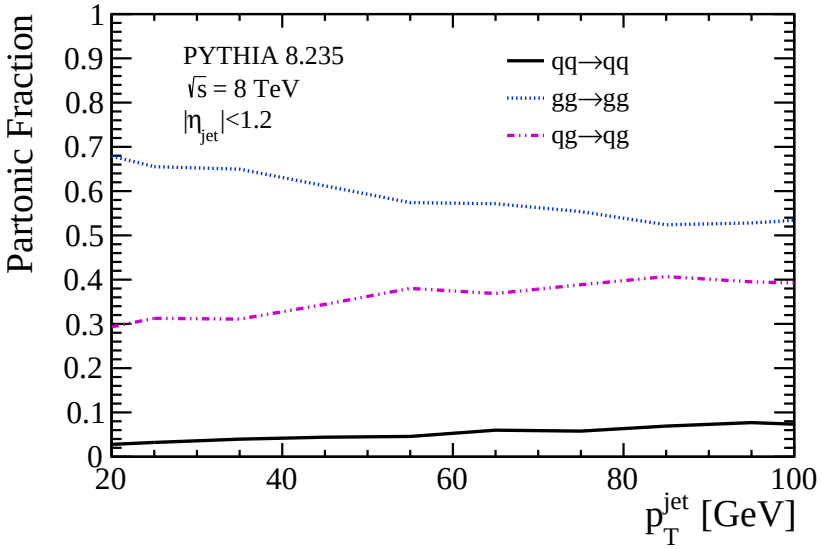

Figure 12: The partonic fractions that contribute to midrapidity inclusive jet production at leading order, according to PYTHIA 8.